NeuroImage: Clinical 22 (2019) 101756

Contents lists available at ScienceDirect

NeuroImage: Clinical

journal homepage: www.elsevier.com/locate/ynicl

More than myelin: Probing white matter differences in prematurity with quantitative T1 and diffusion MRI

Katherine E. Travis[a], Maria R.H. Castro[a], Shai Berman[b], Cory K. Dodson[a], Aviv A. Mezer[b], Michal Ben-Shachar[c,d], Heidi M. Feldman[a,*]

[a] Division of Developmental and Behavioral Medicine, Department of Pediatrics, Stanford University School of Medicine, Stanford, CA, USA
[b] Edmond and Lily Safra Center for Brain Sciences, The Hebrew University of Jerusalem, Jerusalem, Israel
[c] The Gonda Multidisciplinary Brain Research Center, Bar Ilan University, Ramat Gan, Israel
[d] Department of English Literature and Linguistics, Bar Ilan University, Ramat Gan, Israel

ARTICLE INFO

Keywords:
Preterm
Corpus callosum
Fractional anisotropy
Development, myelin

ABSTRACT

Objective: We combined diffusion MRI (dMRI) with quantitative T1 (qT1) relaxometry in a sample of school-aged children born preterm and full term to determine whether reduced fractional anisotropy (FA) within the corpus callosum of the preterm group could be explained by a reduction in myelin content, as indexed by R1 (1/T1) from qT1 scans.

Methods: 8-year-old children born preterm (n = 29; GA 22–32 weeks) and full term (n = 24) underwent dMRI and qT1 scans. Four subdivisions of the corpus callosum were segmented in individual native space according to cortical projection zones (occipital, temporal, motor and anterior-frontal). Fractional anisotropy (FA) and R1 were quantified along the tract trajectory of each subdivision and compared across two birth groups.

Results: Compared to controls, preterm children demonstrated significantly decreased FA in 3 of 4 analyzed corpus callosum subdivisions (temporal, motor, and anterior frontal segments) and decreased R1 in only 2 of 4 corpus callosum subdivisions (temporal and motor segments). FA and RD were significantly associated with R1 within temporal but not anterior frontal subdivisions of the corpus callosum in the term group; RD correlated with R1 in the anterior subdivision in the preterm group only.

Conclusions: Myelin content, as indexed by R1, drives some but not all of the differences in white matter between preterm and term born children. Other factors, such as axonal diameter and directional coherence, likely contributed to FA differences in the anterior frontal segment of the corpus callosum that were not well explained by R1.

1. Introduction

White matter is a dynamic neural structure that changes during development and learning, and is associated with sensorimotor and cognitive functions (Filley and Fields, 2016; Gibson et al., 2014; Wandell, 2016). White matter disturbances are linked to neurological and psychological disorders in adults (Fields, 2008). Disturbances in the typical maturation of white matter have also been reported in several clinical pediatric populations, such as children born preterm. Diffuse white matter injuries observed in the aftermath of preterm birth (PT) have been attributed to the susceptibility of pre-oligodendrocytes, precursors of myelin forming glia, to destruction from hypoxia-ischemia and neuroinflammation during the perinatal period (Back, 2017; Volpe, 2009a) and are associated with poor neurodevelopmental outcomes (Back, 2015; Twilhaar et al., 2017).

Abnormalities in white matter structure can be assessed using diffusion MRI (dMRI). In the newborn period, reduced FA and/or increased mean diffusivity in preterm compared to full term infants (FT) is consistent with the putative pathogenesis and resulting reductions in myelin content (Anjari et al., 2007; Pannek et al., 2014). In older preterm children, FA differences have also been observed (Constable et al., 2008; Dodson et al., 2017; Groeschel et al., 2014; Jo et al., 2012; Travis et al., 2015b). Recent meta-analyses of dMRI in preterm samples found that the genu, body and splenium of the corpus callosum consistently demonstrate significantly reduced FA in preterm as compared to full term children (Li et al., 2015). Pathways of the corpus callosum traverse

Abbreviations: AD, axial diffusivity; CP, Cerebral palsy; CC, corpus callosum; dMRI, diffusion MRI; FA, fractional anisotropy; FT, full term; GA, gestational age; MD, mean diffusivity; PT, preterm; RD, radial diffusivity; qt1, quantitative T1

* Corresponding author at: Medical School Office Building, 1265 Welch Rd. Rm x163, Stanford, CA 94305, USA.
E-mail address: hfeldman@stanford.edu (H.M. Feldman).

https://doi.org/10.1016/j.nicl.2019.101756
Received 11 July 2018; Received in revised form 3 March 2019; Accepted 9 March 2019
Available online 12 March 2019

periventricular white matter regions that show vulnerability to white matter injury in children born preterm (Back, 2017; Volpe, 2009a; Guo et al., 2017). However, studies have yet to establish whether differences seen in the corpus callosum reflect reductions in myelin content or other downstream effects on additional tissue properties that are indexed by dMRI metrics (e.g., crossing fibers, axonal diameter and density) and that may change over development.

In the present study, we combined dMRI with qT1 relaxometry in school-aged children born preterm or term to determine whether reduced FA in corpus callosum subdivisions of the preterm group reflected reduced myelin content. R1, derived from qT1 scans (R1 = 1/T1), is a measure of the longitudinal relaxation rate of water protons in a magnetic field. Rates of R1 (1/s) are most affected by the water content of an image voxel; voxels containing mostly water (e.g., cerebral spinal fluid) exhibit slower (~0.25/s) R1 rates than voxels that are primarily comprised of tissue (e.g., white matter), which exhibit higher (~1.2/s) rates. Rates of R1 are also sensitive to the biophysical composition of tissues within an image voxel, particularly to the tissue composition of myelin and of iron (Gelman et al., 2001; Ogg and Steen, 1998; Stuber et al., 2014). However, within white matter voxels specifically, up to 90% of the R1 signal is explained by variations in myelin content (Stuber et al., 2014). For these reasons, R1 is generally considered to be a useful proxy for tissue myeloarchitecture, particularly in white matter (Antoine et al., 2014).

Recent studies involving clinical populations have begun to use dMRI combined with R1 mapping techniques to dissociate the tissue properties underlying white matter changes observed in neurological disorders, such as multiple sclerosis (Mezer et al., 2013), and psychiatric illnesses, such as anorexia nervosa (Travis et al., 2015a). To our knowledge, the present study is the first to combine qT1 relaxometry with dMRI to interrogate the tissue properties underlying white matter changes observed in the aftermath of preterm birth. Based on the evidence described above, we used these two methods to test our specific hypotheses which were that compared to term children, (1) the current preterm group would replicate evidence for decreased FA in the posterior, body and anterior subdivisions of the corpus callosum as found in many previous studies and summarized in meta-analyses (Li et al., 2015), and (2) that these differences would be explained by decreased R1.

2. Methods

2.1. Participants

Participants were 8 year old preterm (n = 43) and full term (n = 37) children, recruited between 2012 and 2015 as part of a longitudinal study. The qT1 imaging sequence used here became available during the study and was added to the protocol (Mezer et al., 2013). To be included in the present study, participants were required to have useable dMRI and qT1 data and have complete general intelligence measures. Of all the preterm participants in our sample, 14 were excluded from the present analyses because the children underwent a different MRI protocol (n = 2), did not undergo the qT1 imaging protocol (n = 9), or moved too much during scanning (n = 3). Of all term participants in our sample, 13 were not included in the present analyses because they did not undergo the qT1 imaging protocol (n = 4), or moved too much during scanning (n = 9). The final sample thus consisted of 29 preterm (17 males, mean age = 8 years 2.6 months) and 24 full term (13 males, mean age = 8 years 1.7 months) participants. Preterm birth was defined as gestational age (GA) ≤ 32 weeks, the gestational age at which neonates are at greatest risk for white matter injury (Back, 2017). Full term birth was defined as GA ≥ 36 weeks or birth weight ≥ 2500 g. Preterm children were recruited from the High-Risk Infant Follow-Up Clinic at Lucile Packard Children's Hospital Stanford, local parent groups, and surrounding communities in the San Francisco Bay Area. Full term children were recruited through online parent groups, postings in local school newsletters and letters to families who had participated in past research studies in affiliated research laboratories at Stanford University. Exclusion criteria for all participants included neurological factors unrelated to preterm birth that would account for white matter differences amongst participants, including congenital anomalies, active seizure disorder, hydrocephalus or sensorineural hearing loss. Diagnosis of cerebral palsy (CP) was not an exclusion criterion since CP is associated with preterm birth. One preterm participant had mild CP. The experimental protocol was approved by the Stanford University Institutional Review Board #IRB-22233. A parent or legal guardian provided informed written consent and participants were compensated for participation.

Demographic characteristics assessed in this sample included socioeconomic status (SES), as measured using a modified 4-Factor Hollingshead Index (Hollingshead, 1975). General intelligence was also assessed in all participants using the Wechsler Abbreviated Scale of Intelligence (WASI-II), a nationally standardized test of general intellectual abilities (Wechsler and WASI-II, 2011).

Detailed medical information was available for 26 of the 29 preterm participants. Medical complications at birth in the preterm group were: 21 had respiratory distress syndrome; 4 developed bronchopulmonary dysplasia or chronic lung disease; 20 had hyperbilirubinemia; 11 had patent ductus arteriosus; 15 had retinopathy of prematurity or immature retinae; 4 developed necrotizing enterocolitis; 2 were small for GA (≤ 3rd percentile birth weight for GA). In terms of neuroimaging findings during the initial hospitalization, 15 had one or more mildly abnormal findings on head ultrasound or MRI (5 with grade I intraventricular hemorrhage (IVH); 1 with grade II IVH; 1 with small periventricular lesions; 3 with mild white matter injury; 1 with a transient vascular malformation; 3 had enlarged ventricles) and 1 had abnormal findings on head ultrasound or MRI (bilateral grade III IVH). To follow up on the early abnormalities seen in preterm participants on head ultrasound or MRI, a neuroradiologist assessed T1-weighted MRI scans collected as part of the current longitudinal study for 5 features associated with white matter injury (Dodson et al., 2017; Dodson et al., 2018 for description (Dodson et al., 2017; Dodson et al., 2018). Of the 29 preterm subjects, 4 had abnormal T1-weighted scans, including the participant with mild CP.

2.2. MRI acquisition

MRI data were acquired on a 3T Discovery MR750 scanner (General Electric Healthcare, Milwaukee, WI, USA) equipped with a 32-channel head coil (Nova Medical, Wilmington, MA, USA) at the Center for Cognitive and Neurobiological Imaging at Stanford University (www.cni.stanford.edu). All subjects were scanned for research purposes without the use of sedation.

High-resolution T1-weighted (T1w) anatomical images were collected for each subject using an inversion recovery (IR)-prep 3D fast-spoiled gradient (FSPGR) sequence collected in the sagittal plane ($0.9 \times 0.9 \times 0.9\,mm^3$ voxel size). The T1-weighted imaged was used as a common anatomical reference for the alignment of the diffusion tensor image (DTI) maps and qT1 maps.

dMRI data were acquired with a diffusion-weighted, dual-spin echo, echo-planar imaging sequence with full brain coverage. Diffusion weighted gradients were applied at 30 non-collinear directions with a b-value of $1000\,s/mm^2$. In addition, three volumes were acquired at $b = 0$ at the beginning of the scan. We collected 70 axial slices in each participant (TR = 8300 ms; TE = 83.1 ms; FOV = 220 mm; matrix size of 256 × 256, voxel size of $0.8549 \times 0.8549 \times 2\,mm^3$).

qT1 relaxometry was acquired with SPGR echo images acquired at a four different flip angles ($\alpha = 4°$, 10°, 20°, and 30°; TR = 14 ms; TE = 2 ms) (Fram et al., 1987). A voxel size of $0.9375 \times 0.9375 \times 1.5\,mm^3$ was chosen in order to acquire the four SPGR scans in a reasonably short time frame, appropriate for a pediatric clinical sample. To ensure that the scan parameters were similar

between flip angles, SPGR scans were acquired sequentially without breaks or pre-scan normalization. To obtain an unbiased T1 map, we acquired a spin-echo inversion-recovery (SEIR) sequence with echo-planar imaging (EPI) read-out (Stikov et al., 2011) measured at lower resolution. Four inversion times were measured (2400, 1200, 400 and 50 ms; TR = 3 s; TE = 47 ms) with a voxel size of $1.875 \times 1.875 \times 4\,mm^3$. Unbiased T1 maps obtained from SEIR-EPI scans were used to correct for RF transmit bias in the higher-resolution SPGR scans as described and validated by (Mezer et al., 2013; Mezer et al., 2016).

2.3. Image preprocessing

The T1w images were first aligned to the canonical ac-pc orientation.

Diffusion weighted images were pre-processed with Vistasoft (http://github.com/vistalab/vistasoft/mrDiffusion), an open-source software package implemented in MATLAB R2012a (Mathworks, Natick, MA). The dual-spin echo dMRI sequence used here greatly reduces eddy-current distortions (Reese et al., 2003) obviating the need for eddy-current correction. Subject motion during the diffusion weighted scan was corrected using a rigid body alignment algorithm (Rohde et al., 2004). Each diffusion weighted image was registered to the mean of the $b = 0$ images and the mean $b = 0$ image was registered automatically to the participant's T1w image, using a rigid body transformation (implemented in SPM8, http://www.fil.ion.ucl.ac.uk/spm/; no warping was applied). The combined transform that resulted from motion correction and alignment to the T1w anatomy was applied to the raw data once, and the transformed dMRI images were resampled to $2 \times 2 \times 2mm^3$ isotropic voxels. This step was performed because non-isotropic voxels may bias the tensor fit and distort both tracking and measurements of diffusion properties (Oouchi et al., 2007). Diffusion gradient directions were then adjusted to fit the resampled diffusion data (Leemans and Jones, 2009).

For each voxel in the aligned and resampled volume, tensors were fit to the diffusion measurements using a robust least-squares algorithm, Robust Estimation of Tensors by Outlier Rejection (RESTORE), which is designed to remove outliers at the tensor estimation step (Chang et al., 2005). A continuous tensor field was estimated using trilinear interpolation of the tensor elements. The eigenvalue decomposition of the diffusion tensor was calculated and the resulting three eigenvalues ($\lambda1$, $\lambda2$, $\lambda3$) were used to compute fractional anisotropy (FA), radial diffusivity (RD, i.e., the mean of $\lambda2$ and $\lambda3$) and axial diffusivity (AD, i.e., $\lambda1$) (Basser and Pierpaoli, 1996). In the analyses presented here, we focused on FA because it was the metric used in the meta-analysis (Li et al., 2015).

Quantitative T1 maps were calculated using mrQ, (https://github.com/mezera/mrQ), an open-source software package implemented in MATLAB R2012a (Mathworks, Natick, MA). T1 fitting and bias correction was calculated using methods described in (Mezer et al., 2016; Mezer et al., 2013). Briefly, local transmit-coil inhomogeneities are calculated by minimizing the difference between the unbiased T1 map calculated from low-resolution SEIR-*epi* images (Barral et al., 2010) and the T1 map fit from the multiple flip angle SPGR images. Minimization was achieved using a nonlinear least-squares (NLS) solution that assumes transmit-coil inhomogeneities to be smooth in space (Chang et al., 2008). These estimates were then interpolated the to the high-resolution SPGR to generate T1 ($1/T1 = R1$) maps.

To co-register a subject's quantitative T1 images to their dMRI data, we used the Advanced Normalization Tools (ANTs) software package (Avants et al., 2009). This tool was used to warp the qT1 images to the non-diffusion weighted b = 0 images, as these images have relatively similar contrast (Berman et al., 2017). This warping procedure is used to minimize mis-registration errors due to EPI distortions in the dMRI data. EPI distortions were minimal due to the 2× ASSET acceleration used for the readout of the diffusion-weighted images. After applying the diffeomorphic warp, image registration was manually inspected using the mrView software (Tournier et al., 2012). Manual inspection of the aligned images confirmed that the registration was accurate in all subjects. From the qT1 maps, we then derived R1, the inverse of T1 ($R1 = 1/T1$). We chose to analyze R1 for ease of interpretation: higher values of R1 would indicate increases in myelin content just as higher values of FA would be associated with increased myelin content. The validity of the current method has been demonstrated in clinical populations through findings of reduced R1 in patients with multiple sclerosis (Mezer et al., 2013) and adolescent girls with anorexia (Travis et al., 2015a), conditions in which myelin loss is expected.

2.4. Quantification of white matter tissue properties

Automated Fiber Quantification (AFQ; https://github.jyeatman/AFQ), a software package implemented in MATLAB R2012a (Mathworks, Natick, MA), was used to isolate and characterize the corpus callosum in individual native space (Yeatman et al., 2012; Yeatman et al., 2014). In meta-analyses, the genu, body and splenium of the corpus callosum consistently demonstrate significantly decreased FA in preterm compared to full term children (Li et al., 2015). Further, the occipital and temporal segments of the corpus callosum traverse periventricular white matter regions that show vulnerability to injury in preterm children (Back, 2017; Volpe, 2009a; Guo et al., 2017). Therefore, we segmented four subdivisions of the corpus callosum based on the cortical projection zone of the fibers (occipital, temporal, motor, and anterior frontal) and quantified tract profiles of white matter tissue properties along the trajectory of each subdivision. The temporal (CC-temporal) and occipital (CC-occipital) subdivisions of the corpus callosum pass through the splenium and posterior periventricular white matter; the motor subdivision (CC-motor) passes through the body of the corpus callosum; and the anterior frontal (CC-ant-frontal) subdivision passes through the genu of the corpus callosum.

Methods for deterministic tractography, fiber tract identification, segmentation and quantification are described in detail in several previous publications (Dodson et al., 2017; Travis et al., 2015b; Travis et al., 2015a; Yeatman et al., 2012; Travis et al., 2017; Travis et al., 2016). Fig. 1 shows the tracts in a representative preterm participant, including the defining ROIs used to segment each tract from the whole brain tractogram. Tract profiles of tissue parameters (FA and $R1 = 1/T1$) were calculated at 30 equidistant locations (nodes) along the central portion of each fiber tract bounded by the same two ROIs used for tract segmentation. This procedure generated an FA or R1 tract profile that described the variations in either FA or R1 along the central portion of the tract. Tract profiles were also averaged to produce a single mean value for each tract.

2.5. Statistical approach

2.5.1. Group comparisons: demographic and clinical variables

All statistical analyses were performed using SPSS (version 24.0, IBM Corporation, 2014). We computed two-tailed *t*-tests for independent samples for each of the demographic and behavioral measures of age, gestational age, birth weight, SES and general intelligence. We computed a separate chi-square analysis for the one categorical demographic variable of sex. Threshold for significance was set to $p < .05$.

2.5.2. Group comparisons: FA and R1

Group differences in mean tract properties (FA or R1) were first assessed for each subdivision of the corpus callosum by calculating a two-tailed t-test for independent samples. Threshold for significance was set to $p < .05$ and a trend for significance at $p < .1$. We considered the probability of Type I error to be low given that several studies observe reduced FA within the corpus callosum in preterm compared to full term children (Li et al., 2015). For this reason, we did

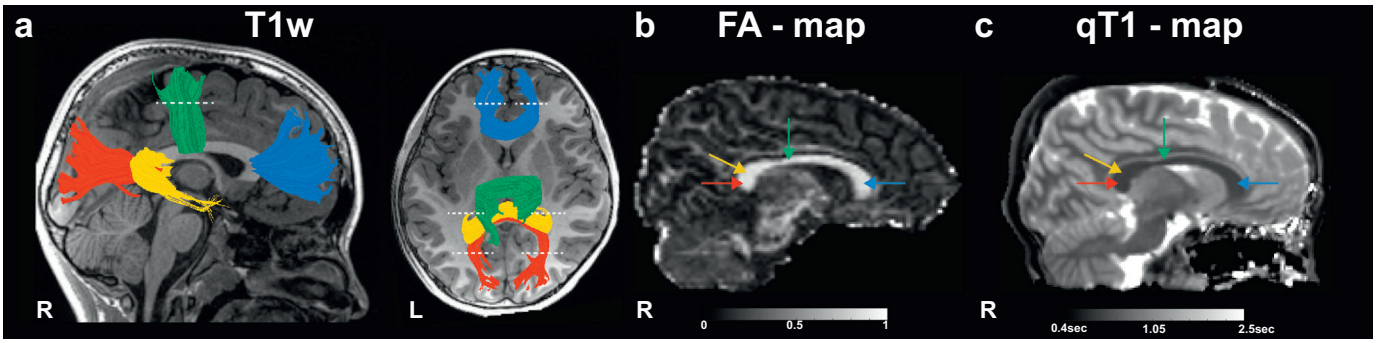

Fig. 1. Tractography of 4 subdivisions of the corpus callosum. (a) Illustrates the following 4 subdivisions of the corpus callosum (CC), in the Splenium: CC-occipital (red), CC-temporal (yellow); Body: CC-motor (green), and Genu: CC-anterior frontal (blue). Tract renderings are displayed on a mid-sagittal and axial T1-weighted (T1w) image from a representative preterm child. Dashed lines represent the location of the regions of interest (ROIs) used to segment each callosal subdivision from the whole-brain fiber group. Colored arrows in panels b and c correspond to tract renderings presented in (a) to indicate the location of each tract within the on a mid-sagittal cross-section of the corpus callosum. Panel (b) displays the location of each subdivision on an FA map of a mid-sagittal cross section of the CC in the same representative preterm child. Panel (c) displays each subdivision on a quantitative T1 (R1 = 1/T1) map of a mid-sagittal cross-section of the same representative preterm child presented in (a).

not correct for the number of comparisons made across the four callosal subdivisions. Effect size of group differences were reported using Cohen's d. Analyses were repeated removing the one participant with cerebral palsy to confirm that group differences were not driven by this child.

We then calculated two-tailed t-tests for independent samples, comparing FA or R1 values of the preterm and full term groups at each location along the tract profile. This analysis was conducted in order to (1) examine whether group differences in FA were accompanied by group differences in R1 in overlapping or non-overlapping locations along the tract profile and (2) confirm that group differences in either FA or R1 were not obscured due to the use of mean tract measures. The analysis of tract profiles utilized a nonparametric permutation-based method to control for 30 comparisons along the tract (Nichols and Holmes, 2002). This procedure produced a critical cluster size for each of the candidate tracts (significant cluster size for all tracts was ≥ 5 locations/nodes). Differences along a tract were considered significant after correction for within tract comparisons if they occurred in a cluster larger than the critical cluster size.

We next performed a series of secondary analyses to further interpret group differences identified in along tract analyses. All secondary analyses described below were performed only for those tracts in which significant group differences identified in along tract analyses survived corrections for multiple comparisons. First, the contributions of axial diffusivity (AD) and radial diffusivity (RD) to group differences observed in FA were examined using a one-way multivariate analysis of variance (MANOVA; (Dodson et al., 2017; Travis et al., 2015b; Dodson et al., 2018). For these analyses group (preterm vs full term) served as the between-subjects variable and mean AD and mean RD computed from significant tract locations served as dependent variables. Significant group effects identified in the MANOVA were then examined with *post-hoc* univariate ANOVAs to establish whether group differences were driven by AD, RD or both.

To explore whether the underlying tissue properties that contributed to individual differences in FA were related to the underlying tissue properties that contributed to individual differences in R1, we performed Pearson correlations between mean FA and mean R1. Pearson correlations were performed based on exploratory analyses that demonstrated normal distributions for the majority of pathways in both FA and mean R1 in the both groups. We restricted the analyses to tract locations where group differences in FA identified in along tract analyses remained significant after correcting for multiple comparisons. We also explored associations of RD and R1 because RD has been shown to be sensitive to variations myelin content (Song et al., 2002). We anticipated a negative association. We again used Pearson correlations because of the normal distributions of RD and R1 for most tracts. We restricted the analyses to the same tract locations as we used for FA-R1 associations. These analyses were performed in each group separately to avoid pseudo-correlations, stemming from group differences.

Follow-up analyses were performed to assess whether group differences in FA or R1 remained significant after controlling variation in Full Scale IQ, which was found to significantly differ between children born preterm and full term in the current sample (Dodson et al., 2017; Travis et al., 2015b; Dodson et al., 2018). These analyses were computed using mean FA or mean R1 computed from significant tract locations entered into a univariate mixed analysis of covariance (mixed-ANCOVA) in which group (preterm vs full term) served as the between subjects factor and Full Scale IQ scores served as the covariate.

3. Results

3.1. Demographic and clinical variables

Results of the group comparisons of demographic and behavioral measures are presented in Table 1. By design, children in the preterm group had significantly decreased GA and birth weight than the full term sample. Children in the preterm group did not differ significantly from the full term group in age, sex, or SES. Children in the preterm group had mean general intelligence standard scores within the normal range but significantly lower than children in the term group.

Table 1
Demographic measures for the preterm and full term sample.

	Preterm (n = 29) mean ± SD or n (%)	Full term (n = 24) mean ± SD or n (%)	t or X^2
Gestational Age (weeks)	29.24 ± 2.18	39.54 ± 1.47	19.69*
Birth Weight (grams)	1278.72 ± 419.07	3365.38 ± 454.16	17.37*
Age (years)	8.22 ± 0.21	8.14 ± 0.14	−1.65
Males	17 (58.6%)	13 (54.2%)	0.12
SES[a]	56.98 ± 9.56	58.42 ± 10.76	0.51
Full 4 IQ SS[b]	105.48 ± 12.50	121.08 ± 12.24	4.56*

SD = standard deviation.
SS = standard score.
SES = socioeconomic status.
* $p < .001$.
[a] Measured using a modified 4-factor Hollingshead Index.
[b] Measured using Wechsler Abbreviated Scale of Intelligence.

Table 2
Birth group differences in mean tract FA and R1 in pathways of the corpus callosum in preterm and full term children.

	FA					R1 (1/s)				
	Preterm mean (95% CI)	Full term mean (95% CI)	*t*	*p*	*d*	Preterm mean (95% CI)	Full term mean (95% CI)	*t*	*p*	*d*
Corpus Callosum										
Occipital	0.70 (0.68–0.71)	0.71 (0.69–0.72)	0.88	0.39	0.2	1.07 (1.04–1.10)	1.10 (1.07–1.12)	1.41	0.17	0.4
Temporal	0.53 (0.50–0.55)	0.55 (0.53–0.57)	2.21	0.04*	0.4	0.94 (0.91–0.98)	1.00 (0.97–1.02)	2.47	0.02*	0.7
Motor	0.54 (0.52–0.56)	0.56 (0.56–0.57)	2.30	0.04*	0.5	1.01 (0.99–1.03)	1.04 (1.02–1.06)	1.93	0.06+	0.6
Anterior Frontal	0.59 (0.58–0.59)	0.60 (0.54–0.57)	1.92	0.08+	0.4	1.10 (1.08–1.12)	1.09 (1.06–1.11)	−0.80	0.43	0.2

CI = confidence interval.
+ $p < .1$.
* $p < .05$.

3.2. Group comparisons: FA and R1

Compared to the full term group, children born preterm demonstrated significantly decreased mean tract FA in 3 of the 4 analyzed subdivisions of the corpus callosum (CC-temporal; CC-motor; CC-anterior frontal; Table 2). Cohen's effect sizes for group FA differences in these three callosal subdivisions were moderate (0.4–0.5; Table 2). Compared to the full term group, children born preterm also demonstrated significantly decreased mean tract R1 in 2 of the 4 analyzed subdivisions of the corpus callosum (CC-temporal; CC-motor; Table 2). Cohen's effect sizes for group R1 differences in these two callosal subdivisions were moderate to large (0.6–0.7; Table 2). No significant birth group differences were observed for mean tract FA and R1 of the CC-occipital (Table 2) or mean tract R1 of the CC-anterior frontal (Table 2). These findings remained the same after removing the one preterm participant with cerebral palsy.

Along tract analyses of tract profiles confirmed that significant decreases in FA observed in the preterm group for the CC-temporal and the CC-motor were accompanied by significant decreases in R1 at several overlapping tract locations (CC-temporal: Fig. 2b,f; CC-motor, Fig. 2c,g). By contrast, significant decreases in FA observed in the preterm group for the CC-anterior frontal were not accompanied by decreased R1 in the preterm group at any tract location (Fig. 2d,h). Finally, in the CC-occipital subdivision, modest decreases were found in FA and R1 values of the preterm group in overlapping and non-overlapping tract regions that did not show significant group differences in mean-tract analyses (Fig. 2a,e).

Secondary analyses demonstrated that decreased FA in the preterm group was driven primarily by significantly increased RD in both the CC-temporal and the CC-anterior frontal (Supplemental Table S1). No birth group differences in AD were observed for either tract.

3.3. Associations between dMRI metrics (FA or RD) and R1

Correlation analyses revealed significant positive associations between mean FA and mean R1 of the CC-temporal in both the preterm ($r_p = 0.73$, $p < .001$; Fig. 3a,b) and full term group ($r_p = 0.65$, $p = .001$; Fig. 3a,c). Significant negative associations were also found between mean RD and mean R1 of the CC-temporal in both the preterm ($r_p = -0.83$, $p < .001$;) and full term group ($r_p = -0.83$, $p < .001$). By contrast, no association was observed between mean FA and mean R1 of the CC-anterior frontal in either the preterm ($r_p = 0.18$, $p = .35$; Fig. 3d,e) or the full term group ($r_p = -0.26$, $p = .22$; Fig. 3d,f). A significant negative association was found between mean RD and mean

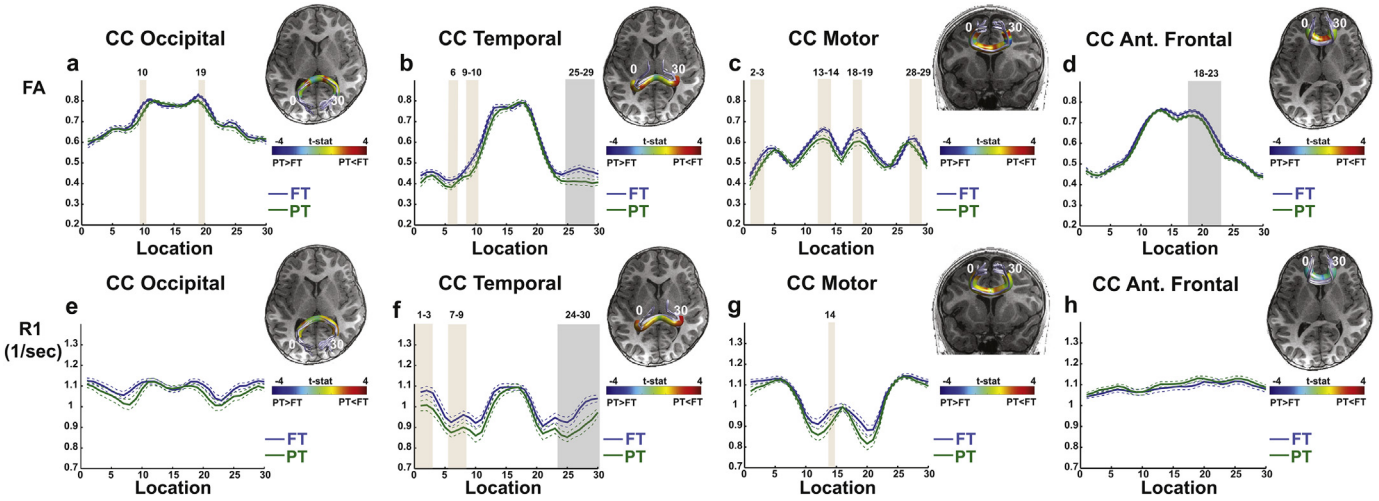

Fig. 2. Preterm children demonstrate significantly decreased FA and decreased R1 in overlapping and non-overlapping regions of 3 subdivisions of the corpus callosum. FA tract profiles (a–d) and R1 tract profiles (e–h) for the preterm (solid green line) and full term (solid blue line) groups are shown for the CC-occipital (a,e), CC-temporal (b,f), CC-motor (c,g) and CC-anterior frontal (d,h). Dashed lines indicate ± 1 standard error of the mean. FA and R1 values are plotted for 30 equidistant locations (nodes) between the two ROIs used to isolate the core of each tract. Shaded gray background indicates tract locations where preterm children demonstrated significantly decreased FA or R1 compared to full term children ($p < .05$, corrected for 30 comparisons by controlling the family-wise error). Shaded tan background indicates tract locations where preterm children demonstrated significantly decreased FA or R1 compared to full term children ($p < .05$, uncorrected). Tract renderings from the same representative preterm subject presented in Fig. 1 are displayed on an axial T1-weighted image next to each tract profile. Magnitude of *t*-tests for independent samples computed to visualize the location of group differences identified in along tract tests are displayed as a colored heat map on a cylinder surrounding tract renderings. Color bar represents magnitude of t statistics. (CC = corpus callosum; Ant = Anterior; PT = preterm; FT = full term; FA = fractional anisotropy).

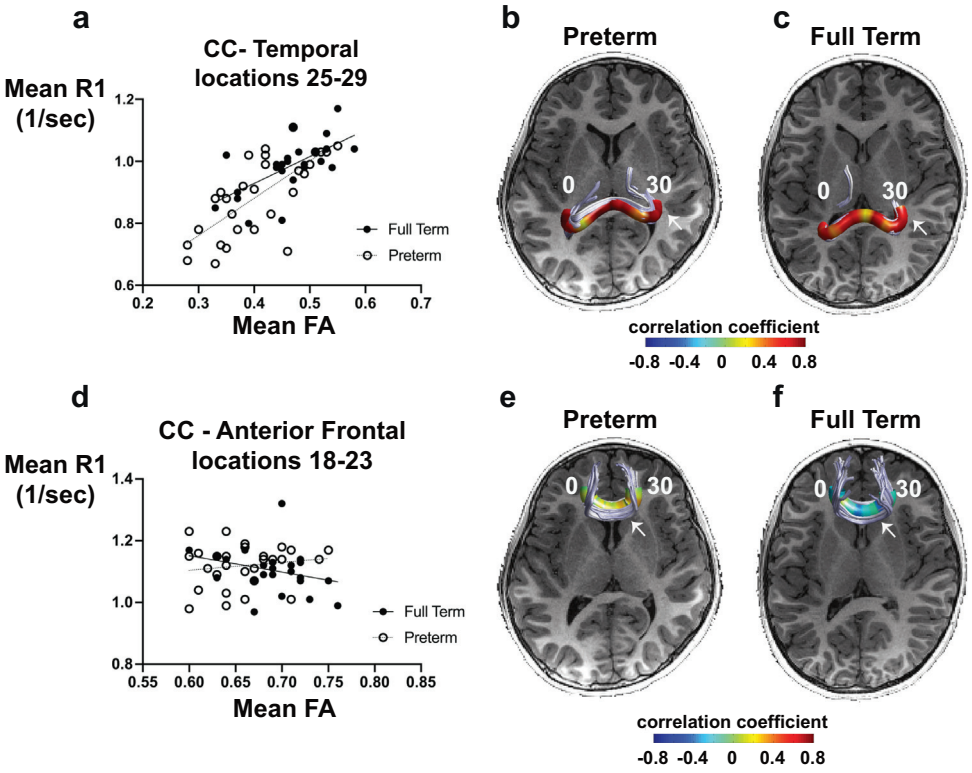

Fig. 3. Decreased FA is associated with decreased R1 in posterior but not anterior tracts of the corpus callosum in preterm and full term children. Scatter plots represent the association between mean FA and mean R1 from significant locations along tract profiles of the CC-temporal (a) and CC-anterior frontal (d). Tract renderings from the same representative preterm subject (b,e) presented in Fig. 1 and a representative full term subject (c,f) are displayed on an axial T1-weighted image next to scatter plots. Strength of correlations between FA and R1 at 30 equidistant locations (nodes) are displayed on a colored cylinder surround tract renderings for the CC-temporal (b,c) and CC-anterior frontal (e,f). White arrows indicate tract location where significant group differences in FA were observed for the CC-temporal (nodes 25–29; b,c) and CC-anterior frontal (nodes 18–23; e,f). Color bar represents Pearson correlation coefficients. (CC = corpus callosum; PT = preterm; FT = full term; FA = fractional anisotropy).

R1 of the CC-anterior frontal in the preterm ($r_p = -0.48$, $p = .009$) but not the full term group ($r_p = 0.21$, $p = .34$).

3.4. IQ

Secondary analyses also demonstrated that birth group differences in the CC-temporal remained significant for both FA ($F(1,50)) = 3.81$, $p = .03$) and R1 ($F(1,50)) = 4.60$, $p = .02$) after co-varying for group differences in IQ. Birth group differences in the CC-anterior frontal for FA also remained significant after co-varying for group differences in IQ ($F(1,50) = 4.17$, $p = .02$).

4. Discussion

In this study of school-aged children born preterm and at term, we employed complementary methods of dMRI and qT1 relaxometry to examine whether birth group differences within the corpus callosum may be explained by reductions in myelin content. We hypothesized that, compared to children born at term, preterm children would show decreased FA within pathways of the corpus callosum consistent with previous research (Li et al., 2015). Group differences in FA were driven by differences in RD, not AD. We also hypothesized that reduced FA would be accompanied by reduced R1, suggestive of reduced myelin content. The first hypothesis was confirmed for the occipital, temporal, motor and anterior frontal subdivisions of the corpus callosum. The second hypothesis was confirmed for the temporal and motor subdivisions, but not for the anterior-frontal subdivision. Further analyses revealed that FA and RD were significantly associated with R1 within posterior but not anterior subdivisions of the corpus callosum, except for RD which correlated with R1 in the preterm group only. Secondary analyses confirmed that group differences in FA or R1 for the temporal and anterior frontal subdivisions were unlikely to be explained by birth group differences in IQ. Taken together, the present findings suggest that white matter abnormalities observed in school-aged children born preterm are likely to involve multiple tissue properties, including, but not limited to myelin. The present findings also suggest that the balance of tissue properties indexed by diffusion metrics may vary across different white matter tracts of the brain and between children born preterm or term.

4.1. Group differences in FA reflect differences in myelin content in posterior CC

Birth group differences in FA observed here for tracts that traverse the posterior corpus callosum (CC-temporal, CC-occipital) are consistent with several previous dMRI studies that have reported decreased FA within regions of the splenium in neonates and children born preterm compared to their term born peers (Jo et al., 2012; Travis et al., 2015b). Effect sizes for group differences in FA were generally comparable to group differences observed in anterior and posterior regions the corpus callosum reported in a previous study of 9–17 year old children and adolescents born preterm and full term that employed similar tractography approaches (Travis et al., 2015b). Here, novel evidence for decreased R1 within the CC-temporal and CC-motor segments is consistent with evidence demonstrating the susceptibility of posterior and periventricular white matter to injuries from hypoxia-ischemia and inflammation in non-human animal models of prematurity (Back, 2017; Volpe, 2009a; Back and Miller, 2014). The present findings suggest dysmaturity of pre-oligodendrocytes beyond the initial perinatal insult may lead to permanent reductions in the amount of myelin in pathways captured by CC-temporal and CC-motor tracts (Back, 2017; Volpe, 2009a; Back and Miller, 2014). Future studies of preterm children that combine dMRI with qT1 methods may clarify the white matter tissue properties directly impacted by specific complications of preterm birth (eg., hypoxia-ischemia, inflammation). Longitudinal studies employing these techniques will be important for specifying the white matter tissue properties that may explain variability observed neurodevelopmental outcomes (Wolke and Meyer, 1999; Anderson et al., 2003) or that may change during development in response to specific environmental experiences or medical treatments.

4.2. Group differences in FA reflect tissue properties other than myelin in anterior CC

Contrary to our initial hypothesis, we observed significantly decreased FA in the preterm compared to the full term group that was not explained by a parallel decrease in R1 within the CC-anterior frontal. Although the present findings are consistent with several previous dMRI studies demonstrating decreased FA within the genu in preterm compared to full term children (Li et al., 2015), we did not find evidence to suggest that decreased levels of FA could be explained by reduced myelin content. Instead, the current findings suggest that additional tissues properties indexed by dMRI metrics that reflect axonal microstructure and fiber organization may account for the present decreases in FA and increased RD, including decreased levels of axonal packing, decreased fiber coherence from increased amounts of fiber crossings, or larger axonal diameters (Basser and Pierpaoli, 1996). Anterior regions belonging to the genu of the corpus callosum contain higher proportions of unmyelinated axons and denser packing of small diameter fibers compared to medial and posterior regions of the corpus callosum (Aboitiz et al., 1992; Stikov et al., 2015). Myelination is also known to proceed slower and peak later in frontal white matter regions compared to medial and posterior brain areas (Kinney et al., 1988; Yakovlev and Lecours, 1967). Such evidence may account for why periventricular and posterior white matter areas demonstrate increased susceptibility to white matter injuries from complications of preterm birth (Back, 2006; Volpe, 2009b). This evidence may also explain why associations between dMRI metrics (FA or RD) and R1 were most evident across birth groups in posterior but not anterior callosal subdivisions.

Deciphering whether decreased FA within anterior corpus callosum pathways reflects decreases in axonal packing or increases in the amount of crossing fibers or axonal diameter will require the application of qT1 imaging and additional sophisticated dMRI analyses for quantifying the amount of fiber crossing and axonal density (e.g., NODDI (Zhang et al., 2012)) and additional MRI imaging methods for quantifying the axonal diameter (e.g., AxCaliber (Assaf et al., 2008)). The combination of these techniques along with qT1 can be used to obtain greater specificity for tissue properties contributing to variations in dMRI that are observed across preterm and full term groups and across and within white matter tracts of the brain. Application of these methods in longitudinal studies will also help to establish how myelination may differ across preterm and full term children.

4.3. Limitations and future directions

Although R1 is strongly related to the amount of myelin within white matter voxels, we cannot rule out the possibility that reduced R1 within the preterm sample may also reflect other tissue properties, such as decreased iron deposition or increased in water content, both possibly arising from axonal loss. However, evidence suggests that the cellular processes that may affect tissue concentrations of water content and of iron deposition may be related to myelination (Barkovich, 2000; Connor and Menzies, 1996; Todorich et al., 2011). The present study also cannot determine whether the observed changes in R1 are the consequence of reduced myelin content beginning in the neonatal period, or secondary changes based on the dysregulation of myelination in the aftermath of preterm birth (eg., axonal loss). Understanding how such white matter tissue properties are impacted in the long term aftermath of preterm birth is likely to require the use of animal models and additional imaging modalities in developing human children.

The present study was based on a convenience sample that was of modest size. We also made no corrections for the four comparisons performed across different callosal segments. However, given that the present findings replicated previous evidence for reduced FA within corpus callosum in preterm compared to full term groups (Li et al., 2015) we expected the likelihood for type I error to be low. Birth group differences observed in FA and R1 in the CC-occipital were modest and would be better tested in larger samples of preterm children than in the current study. Without longitudinal data, we cannot establish whether the observed group differences reflect differences resulting from initial injuries, compensation for injury, or differences in developmental changes. Nevertheless, the present study makes important contributions to understanding white matter tissue properties contributing to altered white matter microstructure observed in older children born preterm.

On-going analyses will examine relationships between dMRI and qT1 metrics in relation to functional outcomes, including individual variation in language and reading outcomes in both children born preterm and at term. The present findings emphasize the importance of including additional metrics based on qT1 measurements in studies of dMRI, in order to aid in the interpretation of group differences identified with dMRI and to understand structure-function associations. The combination of methods is critical to deepening our understanding of the contributions of white matter in development, in health, and in disease.

Acknowledgements

The authors received funding support from the National Institute of Child Health and Human Development (Grant # R01HD069162 [Feldman], 5K99HD084749 [Travis]) and a Young Investigator Award to Dr. Travis, from the Society of Developmental and Behavioral Pediatrics (2014). Funders were not involved in study design, data collection, data analysis, manuscript preparation or publication decisions.

Study funding

NIH (Grant # R01HD069162 [Feldman], 5K99HD084749 [Travis]) and Developmental and Behavioral Pediatrics Young Investigator Award (2014 - Travis). Funding sources had no involvement in the study design, or the collection, analyses and interpretation of data presented in this manuscript.

Data availability statement

Qualified investigators may request anonymized data for purposes of replicating procedures and results from the corresponding author.

Disclosure and conflict of interest statement

Dr. Feldman reports no disclosures or conflicts of interest for any author

Appendix A. Supplementary data

Supplementary data to this article can be found online at https://doi.org/10.1016/j.nicl.2019.101756.

References

Aboitiz, F., Scheibel, A.B., Fisher, R.S., Zaidel, E., 1992. Fiber composition of the human corpus callosum. Brain Res. 598 (1–2), 143–153.
Anderson, P., Doyle, L., Group. VICS, 2003. Neurobehavioral outcomes of school-age children born extremely low birth weight or very preterm in the 1990s. JAMA. 289 (24), 3264–3272.
Anjari, M., Srinivasan, L., Allsop, J.M., Hajnal, J.V., Rutherford, M.A., Edwards, A.D., et al., 2007. Diffusion tensor imaging with tract-based spatial statistics reveals local white matter abnormalities in preterm infants. NeuroImage. 35 (3), 1021–1027.
Antoine, L., Dick, F., Sereno, M.I., W, N., 2014. Using high-resolution quantitative mapping of R1 as an index of cortical myelination. Neuroimage. 93, 176–188.
Assaf, Y., Blumenfeld-Katzir, T., Yovel, Y., Basser, P.J., 2008. AxCaliber: a method for measuring axon diameter distribution from diffusion MRI. Magn. Reson. Med. 59 (6), 1347–1354.
Avants, B.B., Tustison, N., Song, G., 2009. Advanced normalization tools (ANTS). Insight J. 2, 1–35.
Back, S.A., 2006. Perinatal white matter injury: the changing spectrum of pathology and

emerging insights into pathogenetic mechanisms. Ment. Retard. Dev. Disabil. Res. Rev. 12 (2), 129–140.
Back, S.A., 2015. Brain injury in the preterm infant: new horizons for pathogenesis and prevention. Pediatr. Neurol. 53 (3), 185–192.
Back, S.A., 2017. White matter injury in the preterm infant: pathology and mechanisms. Acta Neuropathol. 134 (3), 331–349.
Back, S.A., Miller, S.P., 2014. Brain injury in premature neonates: a primary cerebral dysmaturation disorder? Ann. Neurol. 75 (4), 469–486.
Barkovich, A.J., 2000. Concepts of myelin and myelination in neuroradiology. AJNR Am. J. Neuroradiol. 21 (6), 1099–1109.
Barral, J.K., Gudmundson, E., Stikov, N., Etezadi-Amoli, M., Stoica, P., Nishimura, D.G., 2010. A robust methodology for in vivo T1 mapping. Magn. Reson. Med. 64 (4), 1057–1067.
Basser, P.J., Pierpaoli, C., 1996. Microstructural and physiological features of tissues elucidated by quantitative-diffusion-tensor MRI. J. Magn. Reson. 111 (3), 209–219.
Berman, S., West, K.L., Does, M.D., Yeatman, J.D., Mezer, A.A., 2017. Evaluating g-ratio weighted changes in the corpus callosum as a function of age and sex. NeuroImage 182, 304–313.
Chang, L.C., Jones, D.K., Pierpaoli, C., 2005. RESTORE: robust estimation of tensors by outlier rejection. Magn. Res. Med. 53 (5), 1088–1095.
Chang, L.C., Koay, C.G., Basser, P.J., Pierpaoli, C., 2008. Linear least-squares method for unbiased estimation of T1 from SPGR signals. Magn. Reson. Med. 60 (2), 496–501.
Connor, J.R., Menzies, S.L., 1996. Relationship of iron to oligodendrocytes and myelination. Glia. 17 (2), 83–93.
Constable, R.T., Ment, L.R., Vohr, B.R., Kesler, S.R., Fulbright, R.K., Lacadie, C., et al., 2008. Prematurely born children demonstrate white matter microstructural differences at 12 years of age, relative to term control subjects: an investigation of group and gender effects. Pediatrics. 121 (2), 306–316.
Dodson, C.K., Travis, K.E., Ben-Shachar, M., Feldman, H.M., 2017. White matter microstructure of 6-year old children born preterm and full term. NeuroImage Clin. 16 (Supplement C), 268–275.
Dodson, C.K., Travis, K.E., BL, R., Marchman, V.A., Ben-Shachar, M., Feldman, H.M., 2018. White matter properties associated with pre-reading skills in 6-year-old children born preterm and at term. Dev. Med. Child Neurol. 60 (7), 695–702.
Fields, R.D., 2008. White matter in learning, cognition and psychiatric disorders. Trends Neurosci. 31 (7), 361–370.
Filley, C.M., Fields, R.D., 2016. White matter and cognition: making the connection. J. Neurophysiol. 116 (5), 2093–2104.
Fram, R.J., Herfkens, G.A., Johnson, G.H., Glover, J.P., Shimakawa, A., Perkins, T.G., et al., 1987. Rapid calculation of T1 using variable flip angle gradient refocused imaging. Magn. Res. Imaging. 5, 201–208.
Gelman, N., Ewing, J.R., Gorell, J.M., Spickler, E.M., 2001. EG S. Interregional variation of longitudinal relaxation rates in human brain at 3.0 T: relation to estimated iron and water contents. Magn. Reson. Med. 45 (1), 71–79.
Gibson, E.M., Purger, D., Mount, C.W., Goldstein, A.K., Lin, G.L., Wood, L.S., et al., 2014. Neuronal activity promotes oligodendrogenesis and adaptive myelination in the mammalian brain. Science. 344 (6183), 1252304.
Groeschel, S., Tournier, J.D., Northam, G.B., Baldeweg, T., Wyatt, J., Vollmer, B., et al., 2014. Identification and interpretation of microstructural abnormalities in motor pathways in adolescents born preterm. NeuroImage. 87 (Supplement C), 209–219.
Guo, T., Duerden, E.G., Adams, E., Chau, V., Branson, H.M., Chakravarty, M.M., et al., 2017. Quantitative assessment of white matter injury in preterm neonates: association with outcomes. Neurology. 88 (7), 614–622.
Hollingshead, A., 1975. Four Factor Index of Social Status. Yale University, New Haven, CT.
Jo, H.M., Cho, H.K., Jang, S.H., Yeo, S.S., Lee, E., Kim, H.S., et al., 2012. A comparison of microstructural maturational changes of the corpus callosum in preterm and full-term children: a diffusion tensor imaging study. Neuroradiology. 54 (9), 997–1005.
Kinney, H.C., Brody, B.A., Kloman, A.S., Gilles, F.H., 1988. Sequence of central nervous system myelination in human infancy. II. Patterns of myelination in autopsied infants. J. Neuropathol. Exp. Neurol. 47 (3), 217–234.
Leemans, A., Jones, D.K., 2009. The B-matrix must be rotated when correcting for subject motion in DTI data. Magn. Reson. Med. 61 (6), 1336–1349.
Li, K., Sun, Z., Han, Y., Gao, L., Yuan, L., Zeng, D., 2015. Fractional anisotropy alterations in individuals born preterm: a diffusion tensor imaging meta-analysis. Dev. Med. Child Neurol. 57 (4), 328–338.
Mezer, A., Rokem, A., Berman, S., Hastie, T., Wandell, B.A., 2016. Evaluating quantitative proton-density-mapping methods. Hum. Brain Mapp. 37 (10), 3623–3635.
Mezer, A., Yeatman, J.D., Stikov, N., Kay, K.N., Cho, N.J., Dougherty, R.F., et al., 2013. Quantifying the local tissue volume and composition in individual brains with magnetic resonance imaging. Nat. Med. 19 (12), 1667–1672.
Nichols, T.E., Holmes, A.P., 2002. Nonparametric permutation tests for functional neuroimaging: a primer with examples. Hum. Brain Mapp. 15 (1), 1–25.
Ogg, R.J., Steen, R.G., 1998. Age-related changes in brain T1 are correlated with iron concentration. Magn. Reson. Med. 40 (5), 749–753.
Oouchi, H., Yamada, K., Sakai, K., Kizu, O., Kubota, T., Ito, H., et al., 2007. Diffusion anisotropy measurement of brain white matter is affected by voxel size: underestimation occurs in areas with crossing fibers. AJNR Am. J. Neuroradiol. 28 (6), 1102–1106.
Pannek, K., Scheck, S.M., Colditz, P.B., Boyd, R.N., Rose, S.E., 2014. Magnetic resonance diffusion tractography of the preterm infant brain: a systematic review. Dev. Med. Child Neurol. 56 (2), 113–124.
Reese, T.G., Heid, O., Weisskoff, R.M., Wedeen, V.J., 2003. Reduction of eddy-current-induced distortion in diffusion MRI using a twice-refocused spin echo. Magn. Reson. Med. 49 (1), 177–182.
Rohde, G.K., Barnett, A.S., Basser, P.J., Marenco, S., Pierpaoli, C., 2004. Comprehensive approach for correction of motion and distortion in diffusion-weighted MRI. Magn. Reson. Med. 51 (1), 103–114.
Song, S.-K., Sun, S.-W., Ramsbottom, M.J., Chang, C., Russell, J., AH, C., 2002. Dysmyelination revealed through MRI as increased radial (but unchanged axial) diffusion of water. Neuroimage. 17 (3) (1249–36).
Stikov, N., Campbell, J.S., Stroh, T., Lavelee, M., Frey, S., Novek, J., et al., 2015. In vivo histology of the myelin g-ratio with magnetic resonance imaging. Neuroimage. 118, 397–405.
Stikov, N., Perry, L.M., Mezer, A., Rykhlevskaia, E., Wandell, B.A., Pauly, J.M., et al., 2011. Bound pool fractions complement diffusion measures to describe white matter micro and macrostructure. NeuroImage. 54 (2), 1112–1121.
Stuber, C., Morawski, M., Schafer, A., Labadie, C., Wahnert, M., Leuze, C., et al., 2014. Myelin and iron concentration in the human brain: a quantitative study of MRI contrast. Neuroimage. 93 (Pt 1), 95–106.
Todorich, B., Olopade, J.O., Surguladze, N., Zhang, X., Neely, E., Connor, J.R., 2011. The mechanism of vanadium-mediated developmental hypomyelination is related to destruction of oligodendrocyte progenitors through a relationship with ferritin and iron. Neurotox. Res. 19 (3), 361–373.
Tournier, J.D., Calamante, F., Connelly, A., 2012. MRtrix: diffusion tractography in crossing fiber regions. Int. J. Imaging Syst. Technol. 22, 53–66.
Travis, K.E., Adams, J.N., Ben-Shachar, M., Feldman, H.M., 2015b. Decreased and increased anisotropy along major cerebral white matter tracts in preterm children and adolescents. PLoS One 10 (11), e0142860.
Travis, K.E., Adams, J.N., Kovachy, V.N., Ben-Shachar, M., Feldman, H.M., 2017. White matter properties differ in 6-year old readers and pre-readers. Brain Struct. Funct. 222 (4), 1685–1703.
Travis, K.E., Ben-Shachar, M., Myall, N.J., Feldman, H.M., 2016. Variations in the neurobiology of reading in children and adolescents born full term and preterm. NeuroImage Clin. 11 (Supplement C), 555–565.
Travis, K.E., Golden, N.H., Feldman, H.M., Solomon, M., Nguyen, J., Mezer, A., et al., 2015a. Abnormal white matter properties in adolescent girls with anorexia nervosa. NeuroImage Clin. 9, 648–659.
Twilhaar, E.S., de Kieviet, J.F., Aarnoudse-Moens, C.S., van Elburg, R.M., Oosterlaan, J., 2017. Academic performance of children born preterm: a meta-analysis and meta-regression. Arch. Dis. Child. Fetal Neonatal Ed. 103 (4), F322–F330.
Volpe, J.J., 2009a. Brain injury in premature infants: a complex amalgam of destructive and developmental disturbances. Lancet Neurol. 8 (1), 110–124.
Volpe, J., 2009b. Brain injury in premature infants: a complex amalgam of destructive and developmental disturbances. Lancet Neurol. 40, 110–124.
Wandell, B.A., 2016. Clarifying human white matter. Annu. Rev. Neurosci. 39, 103–128.
Wechsler, D., WASI-II, Hsiao-pin C., 2011. Wechsler Abbreviated Scale of Intelligence. Pearson.
Wolke, D., Meyer, R., 1999. Cognitive status, language attainment, and prereading skills of 6-year-old very preterm children and their peers: the Bavarian longitudinal study. Dev. Med.Child Neurol. 41 (2), 94–109.
Yakovlev, P., Lecours, A., 1967. The myelogenetic cycles of regional maturation of the brain. In: Minkowski, A., Yakovlev, P., Lecours, A.R. (Eds.), Regional Development of the Brain in Early Life, pp. 3–70.
Yeatman, J.D., Dougherty, R.F., Myall, N.J., Wandell, B.A., Feldman, H.M., 2012. Tract profiles of white matter properties: automating fiber-tract quantification. PLoS One 7 (11), e49790.
Yeatman, J.D., Wandell, B.A., Mezer, A.A., 2014. Lifespan maturation and degeneration of human brain white matter. Nat. Commun. 5, 4932.
Zhang, H., Schneider, T., Wheeler-Kingshott, C.A., Alexander, D.C., 2012. NODDI: practical in vivo neurite orientation dispersion and density imaging of the human brain. NeuroImage. 61 (4), 1000–1016.